Available online at www.sciencedirect.com
SCIENCE DIRECT®
Surface Science 577 (2005) L71–L77
SURFACE SCIENCE
www.elsevier.com/locate/susc

Surface Science Letters

Tuning electronic properties of novel metal oxide nanocrystals using interface interactions: MoO_3 monolayers on Au(1 1 1)

Su Ying Quek [a], Monika M. Biener [a,b], Juergen Biener [c,1], Cynthia M. Friend [a,b], Efthimios Kaxiras [a,d,*]

[a] *Division of Engineering and Applied Sciences, Harvard University, Cambridge, MA 02138, USA*
[b] *Department of Chemistry and Chemical Biology, Harvard University, Cambridge, MA 02138, USA*
[c] *Center for Imaging and Mesoscale Structures, Harvard University, Cambridge, MA 02138, USA*
[d] *Department of Physics, Harvard University, Cambridge, MA 02138, USA*

Received 18 September 2004; accepted for publication 11 January 2005
Available online 21 January 2005

Abstract

We report experimental and theoretical investigations of monolayer MoO_3 nanocrystals grown on Au(1 1 1), in contrast to the bilayered structure of the bulk oxide crystal. The Au surface acts as the other half of the bilayer by satisfying local bonding requirements through charge redistribution at the interface. Epitaxy with the Au lattice is achieved through the ability of the Mo–O bonds to rotate about one another. The oxide layer becomes semimetallic as it strains to enhance bonding with the Au substrate. This flexibility of the oxide lattice suggests the possibility of tuning electronic properties of transition metal oxides via interface interactions. The effects of electronic structure on the surface chemistry of oxides are in turn illustrated by H adsorption energetics on MoO_3.

Keywords: Density functional calculations; Scanning tunneling microscopy; Epitaxy; Gold; Molybdenum oxides

Metal oxide nanocrystals on metal surfaces have novel electronic properties due to interface [1,2] and nanoscale [3] effects. The ability to grow such structures in a controllable fashion can open exciting possibilities for practical applications. A case in point is molybdenum oxides, the properties of which depend sensitively on their atomic

* Corresponding author. Address: Department of Physics, Harvard University, 17 Oxford Street, Cambridge, MA 02138, USA. Tel.: +1 617 495 7977/3392; fax: +1 617 496 2545.
E-mail address: kaxiras@cmt.harvard.edu (E. Kaxiras).
[1] Present address: Nanoscale Synthesis and Characterization Laboratory, Lawrence Livermore National Laboratory, 7000 East Ave, Livermore, CA 94550, USA.

0039-6028/$ - see front matter © 2005 Elsevier B.V. All rights reserved.
doi:10.1016/j.susc.2005.01.012

structure and composition. For example, their catalytic activity is determined by the type of oxygen species exposed [4], whilst some oxides exhibit charge density wave instabilities due to the quasi one- and two-dimensional arrangements of oxide octahedra in these systems [5].

MoO_3 nanocrystals were grown on Au(1 1 1) surfaces by both chemical (CVD) and physical vapor deposition (PVD) of Mo, followed by oxidation using NO_2. In the CVD experiments, the surface was typically exposed to 1 L of $Mo(CO)_6$ and 10 L of NO_2 alternatively at 450 K, followed by annealing to 600 K for 1 min after every four cycles of dosing, for a total of 16 cycles. The PVD syntheses were performed at 450–600 K. Typically, 0.3 ML of Mo was deposited at a flux of ~0.25–0.75 ML/min, and oxidized by exposure to 20 L of NO_2. Further experimental details are described elsewhere [6,7].

High resolution scanning tunneling microscopy (STM) and low energy electron diffraction studies indicate that the MoO_3 islands grown by either technique have a $c(4\times2)$ unit cell. Whilst bulk MoO_3 consists of weakly-interacting bilayers [8], STM images reveal that the islands are one monolayer in height, i.e. half of the bilayer found in bulk MoO_3 (Fig. 1(b)). This interesting surface structure has another important ramification: although clean Au(1 1 1) has a herringbone reconstruction [9], STM images indicate that the reconstruction is not continued under the islands (Fig. 1(a)), a feature we adopt in the theoretical model of the system.

The atomic and electronic structure of this system were studied using density functional theory, with the projected augmented wave method [10,11] and Perdew-Wang 91 gradient correction [12], as implemented in VASP [13]. We use a slab model with 6 Au layers in a $c(4\times2)$ supercell, separated by 16.5 Å of vacuum before the oxide is introduced. The MoO_3 monolayer and the top 3 Au layers were relaxed until forces were less than 0.01 eV/Å. Geometry optimizations were performed using a plane-wave cutoff of 400 eV and a 3×3 k-point mesh. A 6×6 mesh did not change the optimized geometry significantly. Energies and charge densities were calculated using a plane-wave cutoff of 500 eV and a 12×12 k-point mesh.

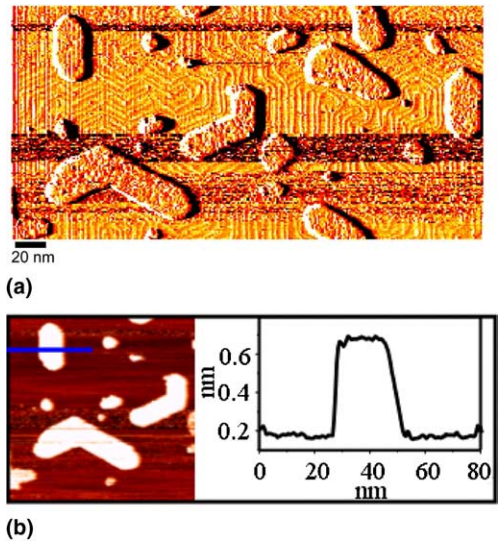

Fig. 1. STM images of MoO_3 islands on Au(1 1 1). The sample was prepared by PVD of 0.3 ML of Mo on Au(1 1 1) at 600 K, and subsequent oxidation by exposure to 20 L of NO_2 at 600 K. The images were collected at room temperature at a sample bias of +2.0 V and a tunneling current of 0.15 nA. (a) Constant height image. The Au herringbone reconstruction runs parallel to the straight island edges, and bends sharply at rough island edges. These bends indicate that the Au(1 1 1) reconstruction is lifted under the MoO_3 islands. (b) Corresponding constant current image of a portion of (a). The line scan on the right is taken along the blue line. It shows that the MoO_3 island has an apparent height of 0.5 nm, in contrast to the height of a bulk bilayer cell which is 1.39 nm [8], thus suggesting that the island consists of a MoO_3 monolayer. (For interpretation of the references in this figure legend, the reader is referred to the web version of this article.)

Such a mesh gave converged total energies in a bulk-terminated Au (1 1 1) surface.

Our calculations reveal that the MoO_3 monolayer (Fig. 2(a)) distorts to fit the Au lattice and has distinct symmetry properties from its bulk analogue (Fig. 2(d)), which served as the guide for our initial oxide structure. In contrast to the bulk case, the MoO_3 monolayer has two non-equivalent planes of reflection and glide symmetry. The slab appears to be composed of MoO_3 units tilting alternately forwards and backwards relative to the surface normal, along the axes of reflection (Fig. 2(b)). Using the notation in Fig. 2, O_{b2} is situated directly above a Au atom, whilst O_{b1} is above a Au bridge site. Mo sits in a 3-fold site, off-centered away from the Au atoms below O_{b2}.

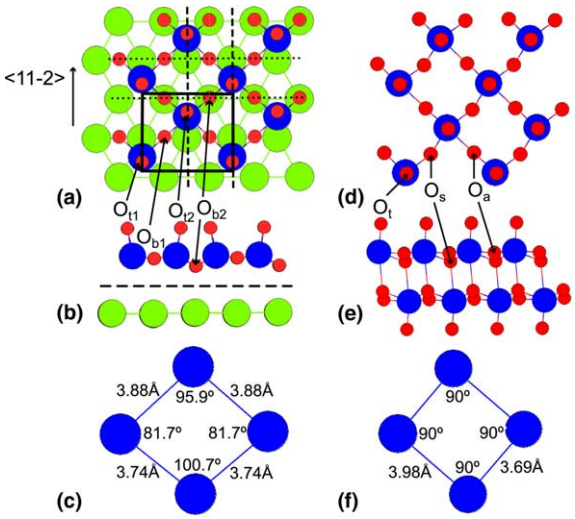

Fig. 2. Atomic structure of MoO_3 slabs. (a) Top view of MoO_3 monolayer on Au. (b) Side view of MoO_3 monolayer on Au. (c) Top view of Mo sublattice in MoO_3 monolayer on Au. (d) Top view showing half a bulk MoO_3 bilayer. (e) Side view of a bulk MoO_3 bilayer. (f) Top view of Mo sublattice in half a bulk MoO_3 bilayer. Blue, red and green circles represent Mo, O and Au atoms respectively. MoO_3 units are close-packed along the diagonal of the $c(4\times2)$ unit cell, indicated by the black box. Dashed and dotted lines in (a) respectively denote planes of reflection and glide symmetry in the oxide monolayer. The view in (b) is that down the glide planes, and shows MoO_3 units tilting backwards and forwards along the axes of reflection. O_{b1} and O_{b2} denote the two inequivalent bridging O atoms in the unit cell of MoO_3 on Au, with O_{b2} nearer to the Au surface than O_{b1}. The terminal O atoms in the MoO_3 monolayer on Au are labeled O_{t1} and O_{t2}. The dashed line in (b) denotes the plane relevant for the plot in Fig. 5. In bulk MoO_3, there are 3 distinct oxygen species, labeled O_t (terminal), O_s (symmetric bridging) and O_a (asymmetric bridging). In the MoO_3 monolayer on Au, the Mo–O bond lengths are 1.69 Å for O_{t1} and O_{t2}, 1.95 Å for O_{b1}, and 1.98 Å for O_{b2}. In bulk MoO_3, the bond lengths are, in Å with experimental values in parentheses, 1.70 (1.67) for Mo–O_t, 1.97 (1.95), 1.97 (1.95), 2.40 (2.33) for each of the 3 Mo–O_s bonds, and 1.77 (1.73), 2.22 (2.25) for the 2 Mo–O_a bonds. Calculated bond lengths in the bulk are within 1–3% of experiment. (For interpretation of the references in this figure legend, the reader is referred to the web version of this article.)

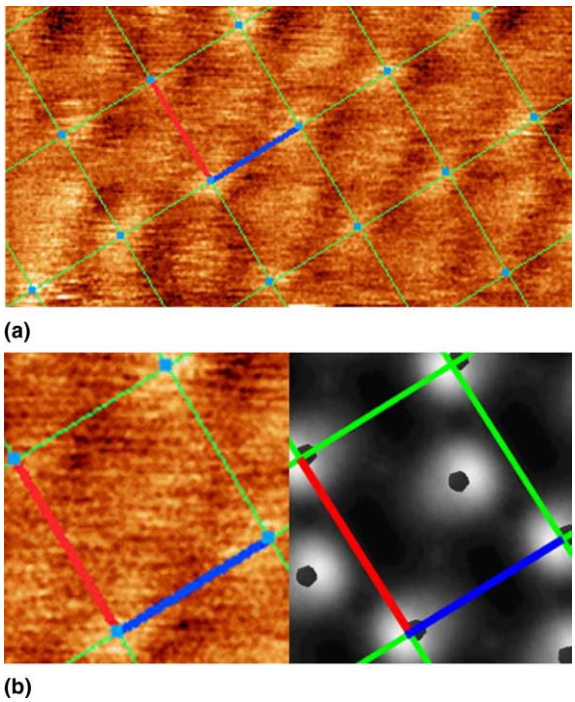

Fig. 3. STM images of the interior of the MoO_3 islands. (a) Experimental STM image, collected at room temperature. (b) Left: Close-up section of experimental STM image in (a). Right: STM simulation corresponding to a tip-sample separation of 1.4 Å. The bias voltages were −0.580 V in both the experiment and the simulation. The tunneling current in the experiment was 25.4 pA. A brighter color represents a more intense current. The green lines show the $c(4\times2)$ unit cells, which are 5.76 Å × 4.99 Å. The bright spots in the experimental images are related to lateral positions of terminal O atoms on the surface, which are marked by black pentagons in the simulation. In each cell, there is a bright spot slightly off-center. In polar co-ordinates with respect to the (x, y) axes (denoted as blue and red in the figure), the off-center spot is at $r = 4.3$ Å, $\theta = 42°$ in the simulation, and $r = 4.1 \pm 0.4$ Å, $\theta = 43 \pm 4°$ in the experiment. (For interpretation of the references in this figure legend, the reader is referred to the web version of this article.)

We performed simulations of the STM images expected for this system based on the Tersoff–Hamann theory [14]. The bright spots in the STM images are found to correspond to lateral positions of terminal O. Within the limits of experimental variance, the relative positions of these spots are the same in theory and experiment (Fig. 3), thus lending strong evidence to the predicted tilting of MoO_3 units.

Phonon frequencies of the MoO_3 monolayer were computed at the Brillouin zone center, using the harmonic approximation. We found only 6 EELS-active [15] phonon modes out of 24 possible ones. The calculated frequencies, with corresponding experimental values in parentheses, are, in cm^{-1}: 1030, 1020 (990), 804 (850), 430 (480), 351

(280) and 160 (not observed). Noting that instrument resolution is about 80 cm^{-1}, and that 160 cm^{-1} is out of the detection range, theoretical and experimental frequencies correspond fairly well, especially since finite-size effects were neglected in the simulation. This correspondence provides further evidence for the predicted symmetry properties.

The preceding results confirm unequivocally that the optimized structure matches the experimental structure of the interior of the MoO_3 monolayer islands on Au(1 1 1), without including defects. It is remarkable that the Mo sublattice from the bulk monolayer distorts by as much as 11° to fit the Au lattice (Fig. 2(c)). Geometrical considerations indicate that the $c(4 \times 2)$ unit cell is in fact the smallest unit cell for which epitaxy can be achieved, if sufficient bonding between Mo atoms through the bridging O bonds is to be preserved. The symmetry properties of the monolayer are also dictated by the symmetries of the Au substrate—the reflection symmetry in the oxide is matched by a reflection symmetry in the Au lattice, and the glide plane symmetry in the oxide corresponds to a similar symmetry in the top Au layer, if its relation to underlying Au layers is ignored. This flexibility of the oxide lattice is achieved by the ability of the Mo–O bonds to rotate about one another: the dihedral angles involving terminal oxygens in the bulk monolayer take the values 0° and 37° (angle O_t–Mo–O_s–Mo in Fig. 2(d)), whereas the corresponding dihedral angles in the relaxed MoO_3 monolayer on Au take values of 7–8°.

Unlike bulk MoO_3 which has a bilayer structure and is semiconducting, the MoO_3 monolayer on the Au surface is semimetallic, as deduced from the density of states (DOS) of the MoO_3/Au system, projected onto the oxide slab (Fig. 4(a)). The MoO_3 monolayer alone has a similar, semimetallic DOS. However, if this monolayer is allowed to relax in the same supercell without the Au substrate, rows of Mo atoms relax alternately towards rows of O_{b1} and O_{b2}, breaking the glide-plane symmetry and the monolayer becomes semiconducting. Analysis of the DOS of the semimetallic MoO_3 monolayer reveals that Fermi level states are localized in the plane of Mo and bridging O

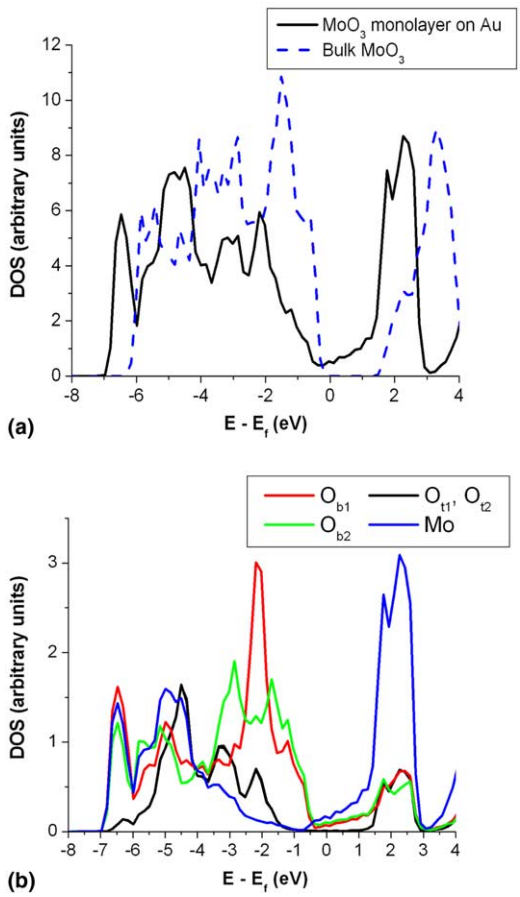

Fig. 4. Projected density of states (DOS) for (a) the MoO_3 monolayer on Au and (b) Mo and the distinct O species in the MoO_3 monolayer on Au. The DOS for bulk MoO_3 is given in the dashed blue line in (a). Unlike bulk MoO_3, the MoO_3 monolayer on Au is semimetallic, with Fermi level states localized in the plane of Mo and bridging O. (For interpretation of the references in this figure legend, the reader is referred to the web version of this article.)

(Fig. 4(b)). These symmetry-degenerate states are split by a Jahn-Teller distortion which leads to a semimetal-to-insulator transition with Mo relaxing towards a pair of bridging O atoms to form stronger bonds.

We expect this oxide monolayer to exhibit interesting surface chemistry because of the relative ease of promoting electrons across the Fermi level in a semimetal. Indeed, H is found to adsorb more strongly than on bulk MoO_3: the binding energies for H at saturation coverage are, in eV,

−3.39, −2.77 and −3.13 on O_t, O_s and O_a respectively in bulk MoO_3 [16], and −3.55, −3.95 and −3.94 on the terminal O, O_{b1} and O_{b2} respectively in the MoO_3 monolayer on Au. In contrast to bulk MoO_3, the bridging oxygens are more stable binding sites for H than the terminal oxygens. This is consistent with the localization of Fermi level states along the plane of bridging O. The adsorption of H on bridging O also provides greater strain relief by breaking up the strained lattice.

The above analysis suggests that the semimetallic character of the MoO_3 monolayer on Au can be attributed to the strained Mo–O bridging bonds. The difference in energy between the relaxed and strained MoO_3 monolayers was 0.15 eV/supercell. The cohesive energy for the MoO_3/Au system, with respect to a relaxed unreconstructed Au(1 1 1) surface and the strained MoO_3 monolayer, was −0.24 eV/supercell. The energy cost of straining the MoO_3 monolayer is therefore overcome by the gain in cohesive energy upon formation of the MoO_3/Au interface. To elucidate the nature of the MoO_3/Au interaction, we plot the difference between the charge density of the MoO_3/Au system, and the sum of charge densities of isolated MoO_3 and Au slabs, frozen in configuration from the joint system (Fig. 5). This reveals that the MoO_3 monolayer induces an electronic charge redistribution above the Au surface. The positively-charged Mo ions draw electron density to the region directly underneath them. Each of these electron clouds is in turn attracted by the nearest Au atom, since Au surface atoms are electron-deficient. In this way, Mo is drawn closer to the Au atom nearest to it. At the same time, the partial negative charges on O_{b2} cause them to be attracted to Au atoms directly beneath them. These interactions together cause the Mo–O_{b2} bridging bonds to strain resulting in semimetallic character. The electronic charge redistribution satisfies local bonding requirements, which allow the Au surface to act as the other half of the MoO_3 bilayer, thereby stabilizing the monolayer nanocrystals. Each Au surface atom is in turn bonded either to an O atom (O_{b2}) or a Mo atom, and as a result, the surface reconstruction under the MoO_3 islands is lifted.

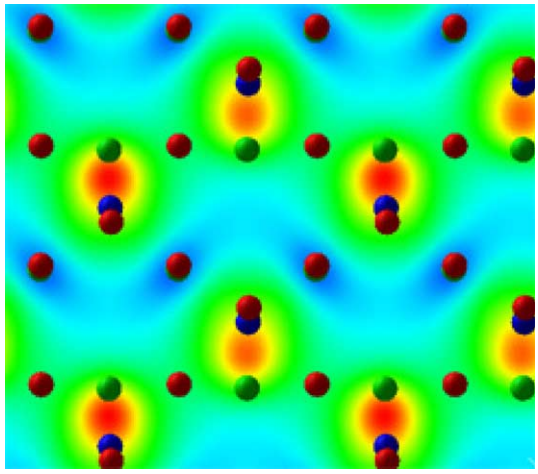

Fig. 5. Charge density difference between the MoO_3/Au system and the sum of charge densities of isolated MoO_3 and Au slabs, frozen in configuration from the joint system. The values are those on a plane mid-way between MoO_3 and Au, as indicated by the dashed line in Fig. 2(b). Blue, red and green spheres denote the lateral positions of Mo, O and Au atoms respectively. Half the Au atoms are hidden directly under O_{b2}. Blue regions, corresponding to charge depletion, occur below O_{b2}, and red regions, corresponding to charge accumulation, are seen between Mo and the nearest Au atoms. Values of the charge density difference range from −0.0093 e/Å^3 to 0.0133 e/Å^3. (For interpretation of the references in this figure legend, the reader is referred to the web version of this article.)

In-situ STM studies suggest that the MoO_3 islands grow via aggregation of MoO_3 molecular species. Earlier theoretical work has shown that induced electrostatic interactions increase the cationic character of Mo as MoO_3 units build up to form bulk MoO_3 [17]. Similarly, in our calculations, the local charge on Mo is larger in the MoO_3 slab on Au than in a single MoO_3 molecule. The increased ionic character upon aggregation of MoO_3 molecular species allows the oxide to polarize the electron gas at the MoO_3/Au interface. Charge redistribution at the interface allows the Au surface to serve as the other half of the MoO_3 bilayer, thus stabilizing the monolayer structures, allowing nucleation and growth. The surface of these islands corresponds to the natural cleavage plane of bulk MoO_3 and has a free energy [18] of only 0.05–0.07 J/m^2. In contrast, Au has a surface free energy [19] of 1.62 J/m^2. Growth of the MoO_3 monolayer is thus driven by both a gain

in interface energy and a reduction in surface free energy.

Interestingly, the long straight edges of the ensuing islands (Fig. 1) run along the $\langle 1\,1\,-2\rangle$ directions of Au, parallel to the herringbone pattern, and not the $\langle -3\,1\,2\rangle$ directions, diagonal to the $c(4\times 2)$ unit cell, along which MoO_3 units are close-packed (Fig. 2(a)). The herringbone pattern is aligned parallel to straight island edges, but tends to form sharp bends at rough island edges. The herringbone pattern has the property of soliton-waves [20]; therefore, absence of Au reconstruction beneath the islands imposes hard-wall boundary conditions on these waves, causing the herringbone pattern to become locally parallel to the island edges. The distinct correlation between straight island edges and the herringbone direction points toward an interplay between the herringbone structure and the MoO_3 islands that affects the overall pattern developed on the surface. Further theoretical and experimental investigation of kinetic effects will substantially clarify the picture.

Conclusion

In this work, we have demonstrated that whilst MoO_3 exists as bilayers in the bulk crystal, MoO_3 monolayer nanocrystals can be grown on the Au(1 1 1) surface. These structures are also distinctly different from previously reported ramified MoO_3 islands grown on Au(1 1 1) [21]. The observed flexibility of dihedral bond angles is likely to be common to many transition metal oxides, especially those with more than one structural phase in the bulk. In fact, it is likely that the growth mechanism proposed herein is general enough so that novel structures of such oxides can be grown on metal surfaces by condensing molecular species, which become increasingly ionic, interacting with the substrate to create a wetting oxide layer. Thin films of some of these oxides have been grown on metal surfaces [22,23]. For example, novel V_xO_y structures were recently grown on Pd(1 1 1) and understood by first principles energetic arguments [23]. Our analysis goes beyond previous studies by showing explicitly how the metallic substrate can induce strain in an oxide monolayer, resulting in changes in the electronic properties of the oxide thereby leading to interesting surface chemistry. These results suggest that the metallic substrate may be used as a handle to tune the electronic properties of interface-mediated oxide structures. The ability to grow crystalline oxide structures epitaxially on metal surfaces thus provides a first step towards synthesizing oxide systems with controllable properties.

Acknowledgement

The calculations were performed on the National Computational Science Alliance IBM P690, under DMR030044. The experimental work was supported by the National Science Foundation, under the Harvard Nanoscale Science and Engineering Center, PHY-011-7795, and the Harvard Materials Research Science and Engineering Center, DMR-0213805, as well as the Department of Energy, Basic Energy Sciences, under FG02-84-ER13289. J.B. acknowledges current support under the auspices of the U. S. Department of Energy by the University of California, Lawrence Livermore National Laboratory under Contract No. W-7405-Eng-48. The authors thank D.-H. Kang and X. Deng for work on EELS and XPS respectively. S.Y.Q. thanks the Singapore Agency for Science, Technology and Research for a graduate fellowship.

References

[1] S.B. Sinnott, E.C. Dickey, Mater. Sci. Eng. R-Rep. 43 (2003) 1.
[2] S. Altieri, L.H. Tjeng, G.A. Sawatzky, Thin Solid Films 400 (2001) 9.
[3] Z.L. Wang, Annu. Rev. Phys. Chem. 55 (2004) 159.
[4] J. Haber, E. Lalik, Catal. Today 33 (1997) 119.
[5] C. Schlenker, Low-Dimensional Electronic Properties of Molybdenum Bronzes and Oxides, Kluwer Academic Publishers, 1989.
[6] M.M. Biener, C.M. Friend, Surf. Sci. 559 (2004) L173.
[7] M.M. Biener, J. Biener, R. Schalek, C.M. Friend, J. Chem. Phys. 121 (2004) 12010.
[8] L. Kihlborg, Arkiv Kemi 21 (1963) 357.
[9] J.V. Barth, H. Brune, G. Ertl, R.J. Behm, Phys. Rev. B 42 (1990) 9307.
[10] G. Kresse, J. Joubert, Phys. Rev. B 59 (1999) 1758.

[11] P.E. Blochl, Phys. Rev. B 50 (1994) 17953.
[12] J.P. Perdew, Y. Wang, Phys. Rev. B 45 (1992) 13244.
[13] G. Kresse, J. Furthmuller, Phys. Rev. B 54 (1996) 11169.
[14] J. Tersoff, D.R. Hamann, Phys. Rev. Lett. 50 (1983) 1998.
[15] H. Ibach, D.L. Mills, Electron Energy Loss Spectroscopy and Surface Vibrations, Academic Press, New York, NY, 1982.
[16] M. Chen, U.V. Waghmare, C.M. Friend, E. Kaxiras, J. Chem. Phys. 109 (1998) 6854.
[17] A. Papakondylis, P. Sautet, J. Phys. Chem. 100 (1996) 10681.
[18] S.H. Overbury, P.A. Bertrand, G.A. Somorjai, Chem. Rev. 75 (1975) 547.
[19] L.Z. Mezey, J. Giber, Jpn. J. Appl Phys 21 (1982) 1569.
[20] M. El-Batanouny, S. Burdick, K.M. Martini, P. Stancioff, Phys. Rev. Lett. 58 (1987) 2762.
[21] Z. Song, T. Cai, Z. Chang, G. Liu, J.A. Rodriguez, J. Hrbek, J. Am. Chem. Soc. 125 (2003) 8059.
[22] S.A. Chambers, Surf. Sci. Rep. 39 (2000) 105.
[23] S. Surnev, G. Kresse, M.G. Ramsey, F.P. Netzer, Phys. Rev. Lett. 87 (2001) 086102-1.